

Can Single Metal Atoms Trapped in Defective h-BN/Cu(111) Improve Electrocatalysis of the H₂ Evolution Reaction?

Daniele Perilli, Cristiana Di Valentin,* and Felix Studt

 Cite This: *J. Phys. Chem. C* 2020, 124, 23690–23698

 Read Online

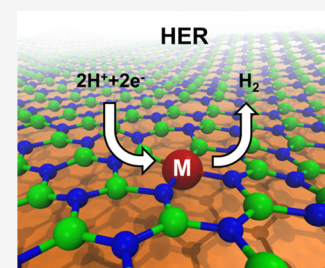
ACCESS |

 Metrics & More

 Article Recommendations

 Supporting Information

ABSTRACT: Metal-supported hexagonal boron nitride monolayers (h-BN/M) are emerging as new potential electrocatalysts for various energy-related oxidation or reduction process. So far, several preparation methods have been developed to introduce, in a controlled way, defects such as vacancies or substitutional heteroatoms. Herein, we investigate by dispersion-corrected density functional theory (DFT) calculations, defective and metal-doped h-BN/Cu(111) systems as electrocatalysts for the hydrogen evolution reaction (HER). By calculating the hydrogen binding energy (ΔG_{*H}) at different coverage conditions, we observe how the interaction between the defective/metal-doped h-BN layer and the Cu(111) substrate plays a key role in tuning the reactivity, leading to a thermoneutral hydrogen adsorption step (i.e., $\Delta G_{*H} \approx 0$). These results could be generalized to other h-BN/M interfaces and may help their rational design for an improved H₂-evolving electrocatalysis.

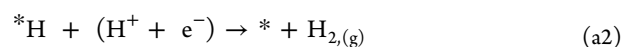


1. INTRODUCTION

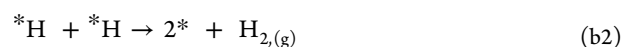
The use of molecular hydrogen (H₂) as an energy carrier is considered a viable alternative to fossil fuels for the energy supply.^{1,2} However, H₂ does not exist naturally on earth and must be produced in a cost-effective way. Nowadays, most of the hydrogen is obtained industrially by steam reforming, which employs fossil fuels, emits carbon dioxide, and produces H₂ of low purity. An alternative clean and renewable route toward the production of pure molecular hydrogen is the direct water splitting,³ which is an uphill reaction but can be conducted electrochemically, thus potentially stemming from renewable sources, such as wind and sun.^{4,5}

Hydrogen evolution is a two-electron reduction process that can follow two possible mechanisms: (a) the *Volmer–Heyrovsky* and (b) the *Volmer–Tafel* paths, which consist of the following sets of reaction steps (in acidic media)

(a) the *Volmer–Heyrovsky* path



(b) the *Volmer–Tafel* path



where * is a catalytic site and *H is a surface-bound hydrogen.

Since both mechanisms share the first electrochemical step (*Volmer*), previous theoretical studies have identified the free binding energy of a hydrogen atom (ΔG_{*H}) as a simple descriptor of the electrocatalytic performance.^{6,7} In fact, according to the *Sabatier* principle, the interaction between

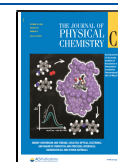
the catalyst and the adsorbate should be “just right”, that is, neither too strong nor too weak. If the interaction is too weak, a high overpotential will be required to bind H and no reaction will take place at a reasonable potential. On the other hand, if the interaction is too strong, the adsorbed H atoms will poison the catalyst and no H₂ will be formed. Thus, the optimum condition is satisfied when the binding of H atoms is close to thermoneutrality, i.e., $\Delta G_{*H} \approx 0$. Taking this simple approximation, it is possible to correlate the electrocatalytic activity with the thermodynamic parameter ΔG_{*H} , which can be calculated rather easily with quantum chemical methods such as DFT. This analysis allowed a rationalization of the reactivity trends among different catalysts (for e.g., expressed through so-called volcano relationships),⁷ but also to identify and predict potential new systems. However, it is worth to highlight how thermoneutrality is a necessary but not sufficient condition for a catalyst to be active for HER.⁸

Currently, state-of-the-art electrocatalysts in acidic media are mainly based on platinum and its alloys, which are rare and costly, and, therefore, not suitable for large-scale use. For all of these reasons, intense scientific efforts are devoted to search for an efficient, inexpensive, stable H₂-evolving electrocatalyst for the HER.⁹ An emerging class of electrocatalysts, which have the potential to meet the above-mentioned requirements, are two-dimensional (2D) materials.^{10–14} For example, (10T0)

Received: July 23, 2020

Revised: September 28, 2020

Published: September 29, 2020



Mo-edges in MoS₂ nanocrystals were found to be active sites for the electrochemical hydrogen evolution, both experimentally^{15,16} and theoretically.^{17–19} Also, in combined experimental and theoretical work, a metal-free hybrid system, made by coupling of graphitic-carbon nitride with nitrogen-doped graphene (g-C₃N₄@NG), was found to be an active electrocatalyst for the hydrogen evolution reaction.²⁰

Another important 2D material that could be of potential interest for electrocatalysis is metal-supported hexagonal boron nitride (h-BN). Although pristine h-BN is intrinsically insulating and inert, when it is chemically modified by dopants, defects, or underlying metal substrates, its reactivity and band gap can be tuned.^{21–28} For example, by combining experiments and DFT calculations, Au-supported h-BN nanosheets were successfully studied for the oxygen reduction reaction (ORR)²⁹ and HER,³⁰ and h-BN edges were proposed to be the active sites for both processes. Recently, Liu et al. experimentally compared the performance of h-BN nanosheets on Cu (h-BN/Cu) and Au (h-BN/Au) and found that the interaction with the underlying metal substrate plays a key role in tuning the electrochemical activity.³¹

An alternative strategy to activate h-BN, and more generally, 2D materials, is by metal doping. These isolated metal atoms could be potentially active sites for several catalytic and electrocatalytic processes, as previously observed in several theoretical studies.^{32–35} Different methods were developed to dope ad hoc 2D materials, such as ion implantation or e-beam evaporation from metal rods.³⁶ However, also impurities and adatoms already present on the metal surface could be incorporated into the 2D layer during its growth by chemical vapor deposition (CVD), as previously proved for epitaxial graphene on an Ni(111) surface.^{37,38}

In our previous studies, we analyzed the electronic interaction between a pristine and defective h-BN monolayer on a Cu(111) substrate,³⁹ and we studied these interfaces as potential electrocatalysts for the oxygen evolution reaction.⁴⁰

In the present work, we investigate whether defective (N and B monoatomic vacancies, and BN diatomic vacancy) and metal-doped (Cu, Ni, Co, and Fe) Cu-supported h-BN systems may be of potential interest for HER. We first analyze the structural and electronic properties and stability of such interfaces. Then, by computing the H-binding energy at different coverage conditions, we evaluate the performance of these h-BN/Cu hybrid systems as electrocatalysts for the hydrogen evolution reaction.

2. COMPUTATIONAL DETAILS

Density functional theory (DFT) calculations were performed using the plane-wave-based Quantum ESPRESSO package (QE).^{41,42} The ultrasoft pseudopotentials⁴³ were adopted to describe the electron–ion interactions with Cu (3d, 4s), Ni (3d, 4s), Co (3d, 4s), Fe (3d, 4s), B (2s, 2p), N (2s, 2p), and H (1s) treated as valence electrons. Energy cutoffs of 30 Ry and 240 Ry (for kinetic energy and charge density expansion, respectively) were used for all calculations. The convergence criterion of 0.026 eV/Å for forces was used during geometry optimization and the convergence criterion for the total energy was set to 10^{−6} Ry. To properly take into account weak interactions, the van der Waals density functional vdW-DF2^{C09x} was used.^{44,45} Spin polarization was considered when required.

For the simulation of h-BN/Cu(111) interfaces, a (6 × 6) supercell with a total of 108 Cu atoms and 72 atoms in the BN

layer was used, resulting in a lattice mismatch of only 0.40%. The Cu(111) surface was modeled by a three-layer slab model with the bottom two layers fixed during the geometry relaxation to mimic a semi-infinite solid. A Monkhorst–Pack⁴⁶ k-points mesh of 3 × 3 × 1 and 9 × 9 × 1 was used for the geometry relaxation and density of states (DOS) evaluation, respectively. To avoid interactions between adjacent periodic images, a vacuum space of about 25 Å was included in the slab model.

The free energies (*G*) of the intermediates (at *T* = 298.15 K) were computed by correcting the electronic energies (*E*) for the zero-point energy (ZPE), heat capacity ($\int C_p dT$), and the vibrational entropic term (*S*_{vib}), calculated as follows

$$G = E + \text{ZPE} + \int C_p dT - TS_{\text{vib}}$$

Vibrational modes were calculated by performing a normal-mode analysis and all 3N degree of freedom of the adsorbates within the harmonic oscillator approximation. Corrections for the ZPE were included by calculating and diagonalizing the dynamical matrix in Gamma point only. For a gas-phase H₂ molecule, the standard tabulated entropy was used.⁴⁷

The electrochemical cell was simulated using the computational hydrogen electrode (CHE) model originally proposed by Nørskov and co-workers.⁴⁸ The climbing image-nudged elastic band (CI-NEB)⁴⁹ method was employed to simulate the *Tafel* step at the Cu-supported defective h-BN, generating the minimum energy path of the reaction step and an evaluation of the energy barrier. A Löwdin population analysis,⁵⁰ as implemented in the QE package, was used to calculate the partial atomic charges. Ball-and-stick models were rendered with Xcrysden software.⁵¹

3. RESULTS AND DISCUSSION

3.1. Structural and Electronic Properties of Metal-doped Defective h-BN/Cu(111) Systems. We previously observed that B vacancies, presenting N-terminated triangular holes in the lattice, can encapsulate Cu adatoms, owing to the large stabilization effect derived from the Cu–N bond formation.³⁹ Therefore, we first considered the monoatomic B vacancy as the “trapping site” for a range of light transition metal atoms (M): Cu, Ni, Co, and Fe. According to the most stable stacking configuration for the h-BN layer on top of the Cu surface, where N/B atoms are in the top/fcc position with respect to the Cu substrate, we considered only the fcc position for the extra metal atom.

We will consider two slightly different situations for the trapped M atoms: (1) the M atom is in the interfacial region, where it is still in contact with the underlying surface but is also bound to the undercoordinated N atoms in the defective h-BN layer (M^{down}@1Vac, Figure 1a); (2) the M atom is exposed toward the vacuum and does not have any contact with the underlying copper substrate (M^{up}@1Vac, Figure 1b).

The M atoms tend to go either up or down because they are quite large and do not perfectly fit in the spatial hole left by the missing B atom. We could not localize a minimum energy structure with the M atom at the same height of the h-BN plane. Therefore, we decided to consider a larger vacancy (diatomic vacancy), where a BN atomic pair is missing, as shown in Figure 1c (M@2Vac). Even for this double vacancy model, all optimized structures show a significant distortion of the 2D layer, and the M atom is always closer to the Cu surface than the h-BN layer.

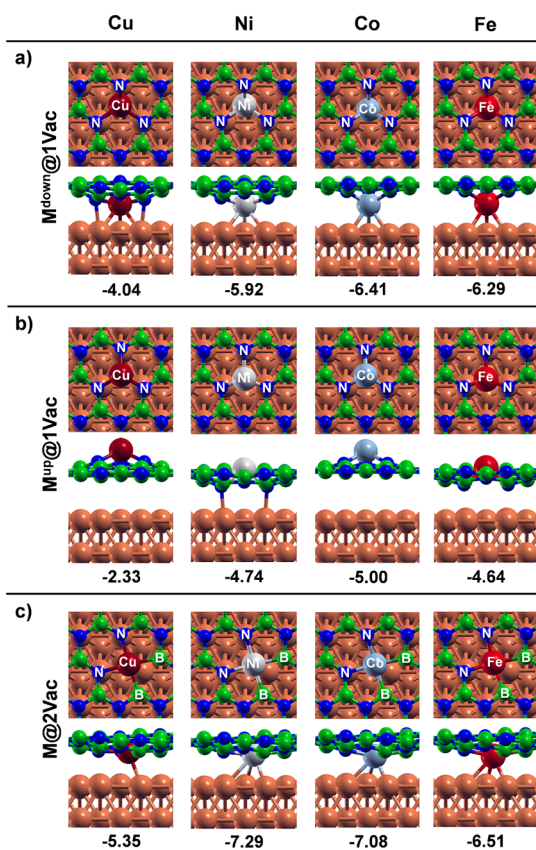


Figure 1. Top and side views for supported metal-doped h-BN in a single B vacancy (1Vac) with the embedded metal in (a) down and (b) up configuration, and into a (c) BN divacancy (2Vac). The corresponding formation energies are reported below each configuration. The formation energies are given relative to the corresponding metal atom in the gas phase. Color coding: Cu surface atoms in orange, N atoms in blue, B atoms in green, and Cu, Ni, Co, and Fe trapped atoms in dark red, gray, cyan, and red, respectively.

Next, we evaluated whether there is an energy cost or gain to go from a defective supported h-BN/Cu layer and trap a single M atom to form the $M@1Vac/2Vac$ structure, according to the following equation

$$E_F = E_{M@1Vac/2Vac} - E_{1Vac/2Vac} - E_{M-atom} \quad (1)$$

where $E_{M@1Vac/2Vac}$, $E_{1Vac/2Vac}$, and E_{M-atom} are the total energies of the M-filled vacancy, empty vacancy, and the isolated metal atom, respectively. This energy change is always negative, although, in the case of $M^{up}@1Vac$, the energy gain is considerably smaller. We rationalize this trend as a consequence of the fact that when the metal is in the up configuration, its interaction with the Cu substrate is completely suppressed. On the contrary, in the down configuration, the stabilization comes from the formation of bonds both with the undercoordinated N atoms from the defective h-BN layer and with the underlying Cu surface atoms.

To get further insight into the nature of the different trapped M atoms, we have analyzed and compared their electronic structure in terms of the total and projected density of states (DOS and PDOS; Figures S1 and S2) of the d states of the embedded M atoms. In the case of the $Cu^{down}@1Vac$ and $Ni^{down}@1Vac$ systems, the d states associated with the single metal atom show a significant broadening due to the strong

coupling with the Cu substrate and have a considerable fraction near the Fermi energy. On the contrary, in the case of the $Co^{down}@1Vac$ and $Fe^{down}@1Vac$ systems, the metal d states show a narrow peak in the proximity of the Fermi energy resembling a similar electronic structure as isolated or single-metal atom catalyst.⁵² Interestingly, only Ni- and Fe-doped systems, in the down atomic configuration, show a residual magnetization after optimization, with a total magnetic moment per cell of $0.69\mu_B$ and $-1.71\mu_B$, respectively. By analyzing the atomic spin density values, such magnetic moment is found to be mainly localized on the trapped metal atoms.

For the systems with a double vacancy, $M@2Vac$ (Figure S2), we note that all projections exhibit less broadening compared to the monovacancy cases, indicating smaller interactions with the Cu substrate: the Cu d states are at a low energy (at least below -2 eV), the Ni and Co d states show a full sharp peak close to the Fermi level (especially, in the case of Co), whereas, in the case of Fe, we observe an empty narrow peak in the α channel (spin-up electrons). Only in the latter case, we found a magnetic ground state, with a total magnetic moment per cell of $-0.65\mu_B$, which is mainly localized on the Fe atom.

We performed a Löwdin population analysis and found that the embedded metal atoms are positively charged due to an electron transfer to the Cu slab. Interestingly, we found that the amount of transferred charge is significantly lower for $M@2Vac$ than for $M@1Vac$ (as shown in Figure 2a).

As pointed out above, the electrochemical stability is another important condition to be satisfied by potential new electrocatalysts. For this reason, we investigated the stability of the trapped M atoms against the dissolution in water, according to a previously employed methodology,^{26,33} as shown in detail in the Supporting Information. Figure 2b,c shows the calculated dissolution potential of trapped metals ($U_{diss(M@V)}$) as a function of the formation energies, as calculated with respect to an isolated (Figure 2b) and bulk-phase (Figure 2c) metal atom. Since the working potential to evolve $H_{2(g)}$ is always negative (with respect to SHE), a positive dissolution potential will guarantee the stability of the trapped metal to its dissolution in water under electrochemical conditions. Therefore, systems in the upper left quadrant of Figure 2 ($U_{diss(M@V)} > 0$ V and formation energy < 0 eV) are promising in terms of stability.

It is interesting to note that all $M^{up}@1Vac$ structures lie in the third quadrant and are therefore not stable, based on the criterion of electrochemical stability. Again, this is due to the absence of the interaction of the trapped metal atom with the underlying Cu substrate, which reduces the overall stability of the system.

In addition to the energy and electrochemical stability, we also considered the activation barrier for Cu and Ni atoms to pass through the B monovacancy, moving between the up ($M^{up}@1Vac$) and down ($M^{down}@1Vac$) structures. As shown in Figure S3, it is interesting to note that all M^{up} structures are not only significantly less stable than their M^{down} counterparts, but the energy barriers from M^{up} to M^{down} are also very small (~ 0.1 eV). M^{up} structures are thus not catalytically relevant and will hence not be considered any further.

To conclude this section, we present the analysis, limited to the case of $M^{down}@1Vac$, of the interaction between M and the three coordinating N atoms. For this, the use of formation energy values, as defined above, is not suitable to compare the

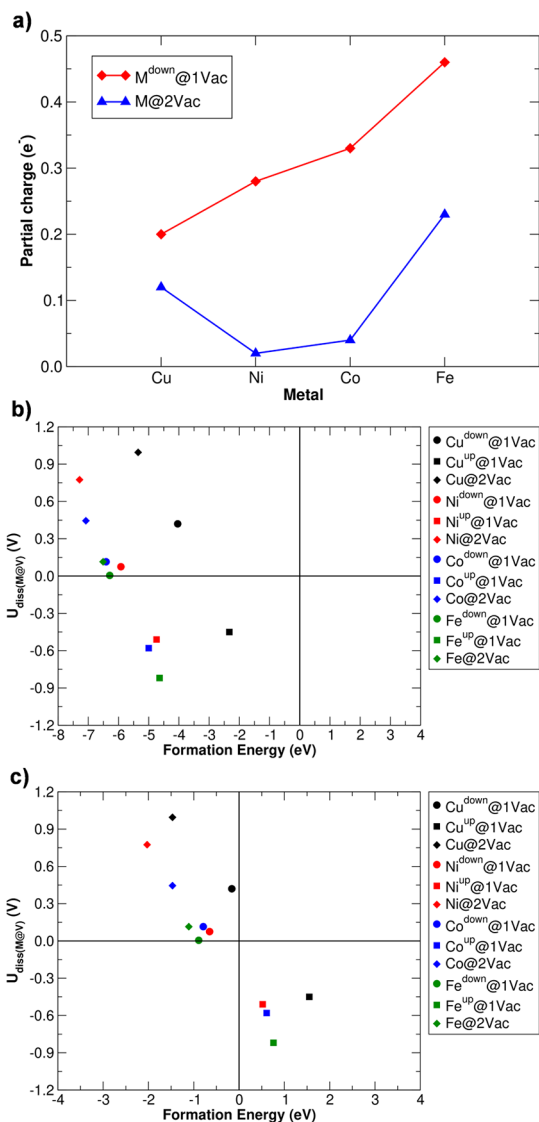


Figure 2. (a) Partial charges of trapped metals for $M^{\text{down}}@1\text{Vac}$ and $M@2\text{Vac}$ systems. Dissolution potentials (with respect to SHE and $\text{pH} = 0$) of trapped metals ($U_{\text{diss}}(\text{M@Vac})$) plotted versus formation energies as calculated with respect to an (b) isolated and (c) bulk-phase metal atom.

strength of the N–M bonds for the following reasons: (1) the formation energy takes the different deformation contributions into account due to both the atomic structural distortions and the change in adhesion strength between h-BN and Cu; (2) in the formation energy, both the contributions of the metal atom interaction with the Cu substrate and with the BN layer are present and cannot be easily separated. The first problem can be solved by employing a simple scheme of energy decomposition, as we used in our previous work.³⁹ As shown in Figure 3a, this decomposition allows one to determine the energy contribution of deformation (positive, ΔE_{def}) and of binding (negative, ΔE_{bind}) to the adsorption energy ($\Delta E_{\text{ads}} = E_{\text{M}@1\text{Vac}} - E_{1\text{Vac}} - E_{\text{M-atom}}$) of $M^{\text{down}}@1\text{Vac}$ (for the values see Table S2). Now, comparing the binding energies (ΔE_{bind}) obtained for the different metal-doped systems, we determined the following order of trapped metal atom stability, from the least to the most stable: Cu (−5.66 eV), Ni (−7.70 eV), Fe (−9.02 eV), and Co (−9.06 eV).

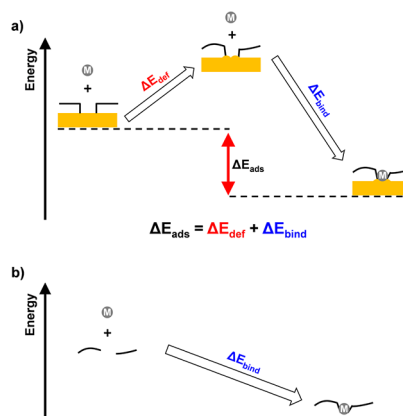


Figure 3. (a) Schematic representation of the energy decomposition analysis for the energy contribution of deformation (positive, ΔE_{def}) and of binding (negative, ΔE_{bind}) to the adsorption energy (negative, ΔE_{ads}) of the metal trapping in the h-B^VN/Cu(111) interface.³⁹ (b) Schematic representation of binding energy contribution derived from the formation of N–M bonds.

As regards the second problem, to roughly estimate only the bonding contribution to the N atoms, we calculated the binding energy of a metal atom trapped in a free-standing h-B^VN layer, which is distorted as when lying over the Cu substrate, according to the scheme reported in Figure 3b. The M–N bond was estimated to increase as follows: −2.24 eV per Cu–N, −2.88 eV per Ni–N, −2.95 eV per Fe–N, and −3.14 eV per Co–N.

3.2. Assessment of the HER on Defective and Metal-Doped h-BN/Cu(111) Interfaces. Defect-free h-BN/Cu(111) was suggested to be a good ORR catalyst based on theoretical calculations.²¹ While we do not necessarily expect that the same is true for HER, we will use h-BN/Cu(111) as our reference system.

We evaluate the stability of the H* intermediates of the HER in terms of Gibbs free energy as

$$\Delta G_{*n\text{H}} = G_{*n\text{H}} - G_* - \frac{n}{2}G_{\text{H}_{2,\text{(g)}}} \quad (2)$$

where $G_{*n\text{H}}$, G_* , and $G_{\text{H}_{2,\text{(g)}}$ are the Gibbs free energies for the catalyst with n hydrogen atoms adsorbed, the catalyst without any hydrogen atom, and an isolated H_2 molecule in the gas phase, respectively. From now on, we will refer to this quantity as the *hydrogen binding energy*.

Another way to evaluate the stability of the *H intermediates is through the *differential hydrogen binding energy*, which is the energy cost or gain to gradually increase the H* coverage and is calculated as follows

$$\Delta G_{*n\text{H}}^{\text{diff}} = G_{*n\text{H}} - G_{*(n-1)\text{H}} - \frac{1}{2}G_{\text{H}_{2,\text{(g)}}} \quad (3)$$

In the case of defect-free h-BN/Cu (Figure S4), we found the electrochemical H adsorption to be unfavorable ($\Delta G_{*1\text{H}} = +1.27$ eV), with the H bonded to a B atom (see Figure S5). This result agrees well with what has been reported from experiments³¹ and suggests that the rather weak interaction between the Cu substrate and the h-BN layer does not alter the activity of h-BN to a great extent ($\Delta G_{*1\text{H}} = +2.41$ eV in the case of free-standing h-BN, Figure S5).

In the following subsections, we present the investigation of the HER mechanism for different defective and metal-doped h-

BN/Cu systems using the computational hydrogen electrode (CHE) model.⁴⁸ For HER, the most optimal electrocatalyst should have a differential hydrogen binding energy close to zero, i.e., $\Delta G_{*H}^{\text{diff}} \approx 0$ eV. As mentioned above, if the interaction is too weak ($\Delta G_{*H}^{\text{diff}} \gg 0$), a high overpotential will be required for the first proton/electron transfer process, whereas, if the interaction is too strong ($\Delta G_{*H}^{\text{diff}} \ll 0$), the adsorbed H binds too strongly, making the second proton/electron transfer step difficult. Thus, the thermoneutrality of this step is a necessary but not sufficient condition for a catalyst to be active for the HER.

3.2.1. Empty Mono- and Diatomic Vacancies. Point defects, such as vacancies, in h-BN are considered to improve its reactivity. When one atom is removed from the h-BN lattice, the monolayer contains some undercoordinated atoms, which become very reactive. Here, we will investigate if this translates into a positive effect on the catalyst activity for HER.

We start considering the case of a boron monovacancy in free-standing h-BN (h-B^VN, Figures 4 and 5a), where the three

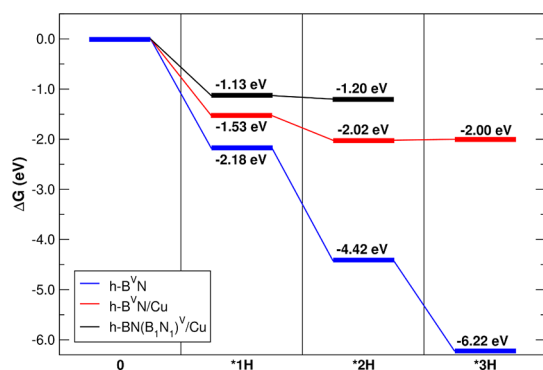


Figure 4. Free-energy diagram (ΔG) for the electrochemical hydrogen adsorption catalyzed by defective Cu-supported h-BN systems and coverage dependence.

nitrogen atoms at the vacancy site are truly undercoordinated (in contrast with the case on a Cu substrate, where they can form bonds with the surface Cu atoms in Figure 5b) and prompt to form new bonds. Because of that, the binding energy for the first H atom added to the free-standing system is higher than in the corresponding Cu-supported h-B^VN. The increase in H coverage by further addition of H atoms leads to comparable energy gains for the various reaction steps (≈ 2 eV). In other words, without an underlying substrate, it is not possible to reach the thermoneutrality since nothing is able to damp the huge energy gain due to the formation of N–H bonds. Nevertheless, the type of the substrate also plays a crucial role to tune the H adsorption, as we can see by comparing the case of h-B^VN supported on Cu(111) with that on Ni(111), which do not agree (Figure S6).

Next, we analyze and compare the boron (h-B^VN/Cu) and the nitrogen (h-BN^V/Cu) monovacancy (red and green lines in Figures 4 and S4, respectively) with the BN divacancy (h-BN(B₁N₁)^V/Cu, black line in Figure 4). The B (N) vacancy induces three undercoordinated N(B) atoms, whereas the BN divacancy gives rise to four undercoordinated N/B atoms (Figures 5b, S5, and 5c, respectively). However, in all cases, the undercoordinated B/N atoms are passivated by Cu surface atoms, forming strong B/N–Cu covalent bonds, as we have shown in detail in a previous work.³⁹

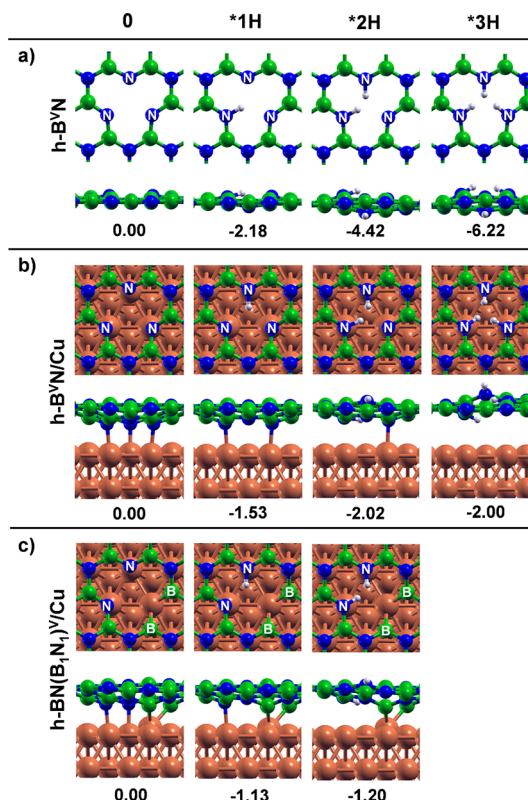


Figure 5. Top and side views of the intermediates of the hydrogen adsorption on (a) free-standing and (b) Cu-supported B monovacancy, and (c) Cu-supported BN divacancy, as shown in Figure 4. The corresponding hydrogen adsorption energies (ΔG_{*nH}) are reported below each structure. Color coding: Cu surface atoms in orange, N atoms in blue, B atoms in green, and H in white.

In the case of h-BN^V/Cu, we calculate $\Delta G_{*1H} = +1.32$ eV (Figure S4) with the H atom that does not bind to an undercoordinated B atom of the vacancy site but to an N atom next to the vacancy, resembling the pristine h-BN/Cu case (see Figure S5).

For h-B^VN/Cu, we calculate a binding energy of -1.53 eV ($\Delta G_{*1H} = \Delta G_{*H}^{\text{diff}}$) for the first coupled proton/electron transfer step. The optimized geometry (second panel in Figure 5b) shows the formation of an N–H bond accompanied by breaking of the previous interfacial N–Cu bond. The energy cost to break one bond is thus compensated by the large energy gain for the formation of the other. While the adsorption of the first hydrogen is rather strong, the calculated differential hydrogen adsorption energy ($\Delta G_{*H}^{\text{diff}}$) decreases with an increase of adsorbed hydrogen and is only -0.49 and $+0.02$ eV for the second and third proton/electron transfer step, respectively. We rationalize this by the cost of breaking the Cu–N bonds and by the steric repulsion between H atoms, which increase with the increase in the number of H atoms. This is confirmed by the observation in Figure 5b that the N–H bonds are pointing out from the BN layer, either up or down, causing some distortion. It is interesting to note in Figure 4 that the differential hydrogen adsorption energy for the third step is calculated to be thermoneutral ($+0.02$ eV). The calculations thus indicate that h-B^VN/Cu is a formidable HER catalyst, with the resting state (i.e., the state before thermoneutral reaction step) having $2H^*$ adsorbed.

For the double vacancy, h-BN(B₁N₁)^V/Cu (black line in Figure 4), our results are similar to the single B vacancy (red

previous section. Therefore, again, we are prone to suggest a possible *Heyrovsky* mechanism, where the H_2 molecule evolves through a direct electrochemical step.

We now move to the case of single metal atoms trapped in a BN divacancy ($M@2Vac$ in Figure 6b). In principle, three possible adsorption sites are available for adsorption: the undercoordinated N atom, the undercoordinated B atom, and the metal atom. We could locate an intermediate where an N–H bond is formed after breaking of one N–M bond (similar to that observed for the $M@1Vac$ above), but its stability, for all metals considered, is always lower ($\approx +0.08/+0.28$ eV) than other adsorption sites. We have indeed found a more favorable intermediate, almost identical among all metals, where H binds in a bridging configuration between the metal and the boron atom (see Figure 6b). To shed more light on the interaction between H and $Fe@2Vac$, in Figure S9, we calculated the charge density difference plot, which proves that the presence of the H atom causes a significant charge redistribution. Here, there is a clear electron charge depletion in the M–B bond and an accumulation between M and H, indicating the formation of an M–H bond. However, some charge accumulation is also located between H and B, indicating that some contribution to the H bond comes from the next B atom.

In Figure 7b, we observe that the first electrochemical H adsorption is unfavorable for Cu- and Ni-doped systems, whereas the differential hydrogen adsorption free energy is close to zero for Co- and Fe-doped systems. We may explain these results, considering the electronic structure details of the different metal-doped systems, as shown in Section 3.1, differently from the case of Cu and Ni trapped metals, where d states are deeper in energy and thus more stable; Co and Fe d states lie in the proximity of the Fermi energy, which, therefore, are expected to be more reactive for M–H bond formation. We have further analyzed the energy-coverage dependence in the case of the Fe- and Co-doped systems (green and blue lines in Figure 7b), as they are both characterized by the first *differential hydrogen binding energy* close to zero. In the latter case ($Fe@2Vac$), we found that a possibility to reach a high coverage at a reasonable energy cost exists. For this system, the activation barrier for the *Tafel* step was found to be +0.96 eV (Figure S10), significantly lower than for the $Ni@1Vac$ case.

4. CONCLUSIONS

In this work, we used dispersion-corrected density functional theory calculations to assess the potential of single metal atoms trapped in defective h-BN on a copper substrate as electrocatalysts for the hydrogen evolution reaction.

Several possible types of interface model systems can be designed when considering various light transition metal atoms, including Cu, Ni, Co, and Fe, as well as various types of h-BN defects (mono- and diatomic vacancies), as we did in this study. For each model system, we have investigated the structural and electronic properties, and we have evaluated the electrochemical stability and activity for HER.

The HER activity was assessed using arguments put forward by the computational hydrogen electrode model, which is the identification of *differential hydrogen adsorption free energy* close to zero, i.e., $\Delta G_{*H}^{diff} \approx 0$ eV, which is the reference for an ideal electrocatalyst. Interestingly, h-BN/Cu(111) layers with mono- or divacancies were found to present differential free adsorption energies close to 0 eV. This is because only the first

hydrogen binds very strongly on these systems, whereas the second (or third) hydrogen atoms are weakly adsorbed.

Next, we investigated how the presence of trapped single metal atoms (Cu, Ni, Co, and Fe) may affect the HER activity. Similarly, as for defective h-BN/Cu(111), metal-doped h-BN/Cu(111) layers were found to present differential free adsorption energies close to 0 eV. Interestingly, the different metal-doped systems differ for the H coverage required to achieve such a condition. In the case of $M@1Vac$ systems, we have observed a correlation between the N–M strength bond and the ΔG_{*H}^{diff} : when the N–M bond is weaker, the H adsorption is stronger (i.e., a more negative ΔG_{*H}^{diff}).

In both cases, Tafel mechanism barriers were calculated to be high ($\approx 1/3$ eV), and therefore we may hypothesize a *Heyrovsky* mechanism, in analogy to what was previously observed for MoS_2 -based catalysts.

Therefore, our results suggest that both defective and single metal-doped h-BN/Cu(111) systems are potentially suitable catalysts for the HER.

Before concluding, we want to compare the systems proposed in this work with MoS_2 -based systems, which are considered as the state-of-the-art two-dimensional catalysts for HER.¹⁶ We note some similarities¹⁷ to our results: (1) the MoS_2 basal plane is inert, whereas HER activity takes place at extended defects, such as Mo-edges; (2) typically, at low coverage, the H atom is too strongly chemisorbed and only the step going from 0.25 to 0.5 ML coverage (corresponding to the differential adsorption free energy, ΔG_{*H}^{diff}) is thermoneutral.

To conclude, the results of the present study could be useful to guide the rational design of h-BN/M interfaces as H_2 -evolving electrocatalysts through their defect engineering and could also stimulate further theoretical as well as experimental investigations in this direction.

■ ASSOCIATED CONTENT

Supporting Information

The Supporting Information is available free of charge at <https://pubs.acs.org/doi/10.1021/acs.jpcc.0c06750>.

Evaluation of the electrochemical stability against the metal dissolution in water for the various $M@1Vac$ and $M@2Vac$ systems; convergence tests for the hydrogen binding energy using three-layer and four-layer models; total (TDOS) and projected (PDOS) density of states of $M@1Vac$ systems; total (TDOS) and projected (PDOS) density of states of $M@2Vac$ systems; energy profile for the flipping of the trapped metal atom in the case of $Cu@1Vac$ and $Ni@1Vac$, with the corresponding ball-and-stick models of the intermediates and transition states; energy contributions of deformation and of binding to the adsorption energy of metal-doped h-BN/Cu systems; the free-energy diagram for the electrochemical H adsorption on pristine and defective h-BN/Cu systems; ball-and-stick models of the intermediates of the H adsorption on pristine and defective h-BN/Cu systems; ball-and-stick models of the intermediates of the H adsorption at different coverages on h-BVN/Ni; the energy profile of the Tafel step for free-standing and Cu-supported h-BVN with the corresponding ball-and-stick models of intermediates and transition states; the energy profile of the Tafel step for $Ni@1Vac$ with the corresponding ball-and-stick models of intermediates and transition state; the charge density

difference plot for Fe@2Vac; and the energy profile of the Tafel step for Fe@2Vac with the corresponding ball-and-stick models of intermediate and transition states (PDF)

AUTHOR INFORMATION

Corresponding Author

Cristiana Di Valentin – Department of Materials Science, University of Milano-Bicocca, 20125 Milano, Italy;
orcid.org/0000-0003-4163-8062;
Email: cristiana.divalentin@unimib.it

Authors

Daniele Perilli – Department of Materials Science, University of Milano-Bicocca, 20125 Milano, Italy

Felix Studt – Institute of Catalysis Research and Technology and Institute for Chemical Technology and Polymer Chemistry, Karlsruhe Institute of Technology (KIT), D-76344 Eggenstein-Leopoldshafen, Germany; orcid.org/0000-0001-6841-4232

Complete contact information is available at:
<https://pubs.acs.org/10.1021/acs.jpcc.0c06750>

Notes

The authors declare no competing financial interest.

ACKNOWLEDGMENTS

This work has been supported by the project “MADAM—Metal Activated 2D cARbon-based platforMs” funded by the MIUR Progetti di Ricerca di Rilevante Interesse Nazionale (PRIN) Bando 2017—grant 2017NYPHN8. F.S. acknowledges the financial support of the Helmholtz Association.

REFERENCES

- (1) Crabtree, G. W.; Dresselhaus, M. S.; Buchanan, M. V. The hydrogen economy. *Phys. Today* **2004**, *57*, 39–44.
- (2) Barreto, L.; Makihira, A.; Riahi, K. The hydrogen economy in the 21st century: a sustainable development scenario. *Int. J. Hydrogen Energy* **2003**, *28*, 267–284.
- (3) Grigoriev, S. A.; Porembsky, V. I.; Fateev, V. N. Pure hydrogen production by PEM electrolysis for hydrogen energy. *Int. J. Hydrogen Energy* **2006**, *31*, 171–175.
- (4) Turner, J. A. Sustainable hydrogen production. *Science* **2004**, *305*, 972–974.
- (5) Seh, Z. W.; Kibsgaard, J.; Dickens, C. F.; Chorkendorff, I. B.; Nørskov, J. K.; Jaramillo, T. F. Combining theory and experiment in electrocatalysis: Insights into materials design. *Science* **2017**, *355*, No. eaad4998.
- (6) Greeley, J.; Jaramillo, T. F.; Bonde, J.; Chorkendorff, I. B.; Nørskov, J. K. Computational high-throughput screening of electrocatalytic materials for hydrogen evolution. *Nat. Mater.* **2006**, *5*, 909–913.
- (7) Nørskov, J. K.; Bligaard, T.; Logadottir, A.; Kitchin, J. R.; Chen, J. G.; Pandelov, S.; Stimming, U. Trends in the exchange current for hydrogen evolution. *J. Electrochem. Soc.* **2005**, *152*, J23–J26.
- (8) Lindgren, P.; Kastlunger, G.; Peterson, A. A. A Challenge to the G~0 Interpretation of Hydrogen Evolution. *ACS Catal.* **2020**, *10*, 121–128.
- (9) Vesborg, P. C.; Seger, B.; Chorkendorff, I. B. Recent development in hydrogen evolution reaction catalysts and their practical implementation. *J. Phys. Chem. Lett.* **2015**, *6*, 951–957.
- (10) Wang, H.; Tsai, C.; Kong, D.; Chan, K.; Abild-Pedersen, F.; Nørskov, J. K.; Cui, Y. Transition-metal doped edge sites in vertically aligned MoS₂ catalysts for enhanced hydrogen evolution. *Nano Res.* **2015**, *8*, 566–575.
- (11) Deng, D.; Novoselov, K. S.; Fu, Q.; Zheng, N.; Tian, Z.; Bao, X. Catalysis with two-dimensional materials and their heterostructures. *Nat. Nanotechnol.* **2016**, *11*, 218.
- (12) Jin, H.; Guo, C.; Liu, X.; Liu, J.; Vasileff, A.; Jiao, Y.; Qiao, S. Z.; et al. Emerging two-dimensional nanomaterials for electrocatalysis. *Chem. Rev.* **2018**, *118*, 6337–6408.
- (13) Tang, Q.; Jiang, D. E. Mechanism of hydrogen evolution reaction on 1T-MoS₂ from first principles. *ACS Catal.* **2016**, *6*, 4953–4961.
- (14) Zheng, Y.; Jiao, Y.; Li, L. H.; Xing, T.; Chen, Y.; Jaroniec, M.; Qiao, S. Z. Toward design of synergistically active carbon-based catalysts for electrocatalytic hydrogen evolution. *ACS Nano* **2014**, *8*, 5290–5296.
- (15) Jaramillo, T. F.; Jørgensen, K. P.; Bonde, J.; Nielsen, J. H.; Hørch, S.; Chorkendorff, I. Identification of active edge sites for electrochemical H₂ evolution from MoS₂ nanocatalysts. *Science* **2007**, *317*, 100–102.
- (16) Kibsgaard, J.; Chen, Z.; Reinecke, B. N.; Jaramillo, T. F. Engineering the surface structure of MoS₂ to preferentially expose active edge sites for electrocatalysis. *Nat. Mater.* **2012**, *11*, 963.
- (17) Hinnemann, B.; Moses, P. G.; Bonde, J.; Jørgensen, K. P.; Nielsen, J. H.; Hørch, S.; Nørskov, J. K.; et al. Biomimetic hydrogen evolution: MoS₂ nanoparticles as catalyst for hydrogen evolution. *J. Am. Chem. Soc.* **2005**, *127*, 5308–5309.
- (18) Tsai, C.; Chan, K.; Nørskov, J. K.; Abild-Pedersen, F. Theoretical insights into the hydrogen evolution activity of layered transition metal dichalcogenides. *Surf. Sci.* **2015**, *640*, 133–140.
- (19) Huang, Y.; Nielsen, R. J.; Goddard, W. A., III; Soriaga, M. P. The reaction mechanism with free energy barriers for electrochemical dihydrogen evolution on MoS₂. *J. Am. Chem. Soc.* **2015**, *137*, 6692–6698.
- (20) Zheng, Y.; Jiao, Y.; Zhu, Y.; Li, L. H.; Han, Y.; Chen, Y.; Qiao, S. Z.; et al. Hydrogen evolution by a metal-free electrocatalyst. *Nat. Commun.* **2014**, *5*, No. 3783.
- (21) Koitz, R.; Nørskov, J. K.; Studt, F. A systematic study of metal-supported boron nitride materials for the oxygen reduction reaction. *Phys. Chem. Chem. Phys.* **2015**, *17*, 12722–12727.
- (22) Hu, G.; Wu, Z.; Dai, S.; Jiang, D. E. Interface Engineering of Earth-Abundant Transition Metals Using Boron Nitride for Selective Electroreduction of CO₂. *ACS Appl. Mater. Interfaces* **2018**, *10*, 6694–6700.
- (23) Lyalin, A.; Nakayama, A.; Uosaki, K.; Taketsugu, T. Functionalization of monolayer h-BN by a metal support for the oxygen reduction reaction. *J. Phys. Chem. C* **2013**, *117*, 21359–21370.
- (24) Lyalin, A.; Nakayama, A.; Uosaki, K.; Taketsugu, T. Theoretical predictions for hexagonal BN based nanomaterials as electrocatalysts for the oxygen reduction reaction. *Phys. Chem. Chem. Phys.* **2013**, *15*, 2809–2820.
- (25) Lyalin, A.; Nakayama, A.; Uosaki, K.; Taketsugu, T. Adsorption and catalytic activation of the molecular oxygen on the metal supported h-BN. *Top. Catal.* **2014**, *57*, 1032–1041.
- (26) Back, S.; Siahrostami, S. Noble metal supported hexagonal boron nitride for the oxygen reduction reaction: a DFT study. *Nanoscale Adv.* **2019**, *1*, 132–139.
- (27) Zhu, W.; Wu, Z.; Foo, G. S.; Gao, X.; Zhou, M.; Liu, B.; Li, H.; et al. Taming interfacial electronic properties of platinum nanoparticles on vacancy-abundant boron nitride nanosheets for enhanced catalysis. *Nat. Commun.* **2017**, *8*, No. 15291.
- (28) Fu, Q.; Meng, Y.; Fang, Z.; Hu, Q.; Xu, L.; Gao, W.; Lu, F.; et al. Boron nitride nanosheet-anchored pd–fe core–shell nanoparticles as highly efficient catalysts for Suzuki–Miyaura coupling reactions. *ACS Appl. Mater. Interfaces* **2017**, *9*, 2469–2476.
- (29) Uosaki, K.; Elumalai, G.; Noguchi, H.; Masuda, T.; Lyalin, A.; Nakayama, A.; Taketsugu, T. Boron nitride nanosheet on gold as an electrocatalyst for oxygen reduction reaction: theoretical suggestion and experimental proof. *J. Am. Chem. Soc.* **2014**, *136*, 6542–6545.
- (30) Uosaki, K.; Elumalai, G.; Dinh, H. C.; Lyalin, A.; Taketsugu, T.; Noguchi, H. Highly efficient electrochemical hydrogen evolution

reaction at insulating boron nitride nanosheet on inert gold substrate. *Sci. Rep.* **2016**, *6*, No. 32217.

(31) Liu, D. Q.; Tao, B.; Ruan, H. C.; Bentley, C. L.; Unwin, P. R. Metal support effects in electrocatalysis at hexagonal boron nitride. *Chem. Commun.* **2019**, *55*, 628–631.

(32) Mao, K.; Li, L.; Zhang, W.; Pei, Y.; Zeng, X. C.; Wu, X.; Yang, J. A theoretical study of single-atom catalysis of CO oxidation using Au embedded 2D h-BN monolayer: a CO-promoted O₂ activation. *Sci. Rep.* **2015**, *4*, No. 5441.

(33) Back, S.; Kulkarni, A. R.; Siahrostami, S. Single Metal Atoms Anchored in Two-Dimensional Materials: Bifunctional Catalysts for Fuel Cell Applications. *ChemCatChem* **2018**, *10*, 3034–3039.

(34) Cui, Q.; Qin, G.; Wang, W.; Sun, L.; Du, A.; Sun, Q. Mo-doped boron nitride monolayer as a promising single-atom electrocatalyst for CO₂ conversion. *Beilstein J. Nanotechnol.* **2019**, *10*, 540–548.

(35) Tan, X.; Tahini, H. A.; Arandiyani, H.; Smith, S. C. Electrocatalytic Reduction of Carbon Dioxide to Methane on Single Transition Metal Atoms Supported on a Defective Boron Nitride Monolayer: First Principle Study. *Adv. Theory Simul.* **2019**, *2*, No. 1800094.

(36) Auwärter, W. Hexagonal boron nitride monolayers on metal supports: Versatile templates for atoms, molecules and nanostructures. *Surf. Sci. Rep.* **2019**, *74*, 1–95.

(37) Patera, L. L.; Bianchini, F.; Africh, C.; Dri, C.; Soldano, G.; Mariscal, M. M.; Comelli, G.; et al. Real-time imaging of adatom-promoted graphene growth on nickel. *Science* **2018**, *359*, 1243–1246.

(38) Carnevali, V.; Patera, L. L.; Prandini, G.; Jugovac, M.; Modesti, S.; Comelli, G.; Africh, C.; et al. Doping of epitaxial graphene by direct incorporation of nickel adatoms. *Nanoscale* **2019**, *11*, 10358–10364.

(39) Perilli, D.; Selli, D.; Liu, H.; Bianchetti, E.; Di Valentin, C. h-BN Defective Layers as Giant N-Donor Macrocycles for Cu Adatom Trapping from the Underlying Metal Substrate. *J. Phys. Chem. C* **2018**, *122*, 23610–23622.

(40) Perilli, D.; Selli, D.; Liu, H.; Di Valentin, C. Computational Electrochemistry of Water Oxidation on Metal-Doped and Metal-Supported Defective h-BN. *ChemSusChem* **2019**, *12*, 1995–2007.

(41) Giannozzi, P.; Baroni, S.; Bonini, N.; Calandra, M.; Car, R.; Cavazzoni, C.; Dal Corso, A.; et al. QUANTUM ESPRESSO: a modular and open-source software project for quantum simulations of materials. *J. Phys.: Condens. Matter* **2009**, *21*, No. 395502.

(42) Giannozzi, P.; Andreussi, O.; Brumme, T.; Bunau, O.; Nardelli, M. B.; Calandra, M.; Colonna, N.; et al. Advanced capabilities for materials modelling with Quantum ESPRESSO. *J. Phys.: Condens. Matter* **2017**, *29*, No. 465901.

(43) Vanderbilt, D. Soft self-consistent pseudopotentials in a generalized eigenvalue formalism. *Phys. Rev. B: Condens. Matter Mater. Phys.* **1990**, *41*, 7892.

(44) Lee, K.; Murray, ÉD.; Kong, L.; Lundqvist, B. I.; Langreth, D. C. Higher-accuracy van der Waals density functional. *Phys. Rev. B: Condens. Matter Mater. Phys.* **2010**, *82*, No. 081101.

(45) Hamada, I.; Otani, M. Comparative van der Waals density-functional study of graphene on metal surfaces. *Phys. Rev. B: Condens. Matter Mater. Phys.* **2010**, *82*, No. 153412.

(46) Monkhorst, H. J.; Pack, J. D. Special points for Brillouin-zone integrations. *Phys. Rev. B: Condens. Matter Mater. Phys.* **1976**, *13*, 5188.

(47) <http://www.webbook.nist.gov> (23/07/2020).

(48) Nørskov, J. K.; Rossmeisl, J.; Logadottir, A.; Lindqvist, L. R. K. J.; Kitchin, J. R.; Bligaard, T.; Jonsson, H. Origin of the overpotential for oxygen reduction at a fuel-cell cathode. *J. Phys. Chem. B* **2004**, *108*, 17886–17892.

(49) Henkelman, G.; Uberuaga, B. P.; Jónsson, H. A climbing image nudged elastic band method for finding saddle points and minimum energy paths. *J. Chem. Phys.* **2000**, *113*, 9901–9904.

(50) Löwdin, P.-O. Quantum theory of many-particle systems. I. Physical interpretations by means of density matrices, natural spin-orbitals, and convergence problems in the method of configurational interaction. *Phys. Rev.* **1955**, *97*, 1474.

(51) Kokalj, A. XCrySDen—a new program for displaying crystalline structures and electron density. *J. Mol. Graphics Modell.* **1999**, *17*, 176–179.

(52) Wang, Y.; Mao, J.; Meng, X.; Yu, L.; Deng, D.; Bao, X. Catalysis with two-dimensional materials confining single atoms: concept, design, and applications. *Chem. Rev.* **2019**, *119*, 1806–1854.